g factors of the low-lying states in ^{106}Pd: Examination of the vibrational character of ^{106}Pd

G. Gürdal,[1] G. J. Kumbartzki,[1] N. Benczer-Koller,[1] Y. Y. Sharon,[1] L. Zamick,[1] S. J. Q. Robinson,[2] T. Ahn,[3] R. Casperson,[3] A. Heinz,[3] G. Ilie,[3] J. Qian,[3] V. Werner,[3] E. Williams,[3] R. Winkler,[3] and D. McCarthey[3,4]

[1]*Department of Physics and Astronomy, Rutgers University, New Brunswick, New Jersey 08903, USA*

[2]*Millsaps College, Jackson, Mississippi 39210, USA*

[3]*A. W. Wright Nuclear Structure Laboratory, Yale University, New Haven, Connecticut 06520, USA*

[4]*Department of Physics, University of Surrey, Guildford, Surrey, United Kingdom*

(Received 15 October 2010; published 3 December 2010)

The transient field (TF) technique in inverse kinematics was used to measure the g factors of the low lying 2_1^+, 4_1^+, and 2_2^+ states in ^{106}Pd. The g factor of the 4_1^+ state was determined and the $g(2_1^+)$ and $g(2_2^+)$ factors were remeasured. The values of $g(2_1^+)$ and $g(2_2^+)$ had been determined earlier in integral perturbed angular correlation (IPAC) experiments and the value of the former served to calibrate the TF. The three g factors, $g(2_1^+)$, $g(2_2^+)$, and $g(4_1^+)$, agree with each other and with the collective Z/A value. The uncertainties in the $g(2_2^+)$ and $g(4_1^+)$ factors remain fairly large in spite of long measuring times because of the weak excitation of the two-phonon states. The lifetimes of the 2_2^+ and 4_1^+ states were newly determined from line-shape fits.

DOI: 10.1103/PhysRevC.82.064301 PACS number(s): 21.10.Ky, 21.10.Tg, 25.70.De, 27.60.+j

I. INTRODUCTION

The simple pure-harmonic collective quadrupole-phonon vibrational model [1] makes definite predictions about the low-energy structure of even-even nuclei. Some of these predictions are summarized by Fig. 1(a).

In the pure vibrational model the excitation-energy of the degenerate two-phonon 0_2^+, 2_2^+, and 4_1^+ triplet is twice that of the one-phonon 2_1^+ singlet state. The $E2$ transitions are expected to be collective and have double-digit $B(E2)$ values in Weisskopf units. A two-phonon transition from the 2_2^+ to the 0_1^+ state is forbidden, as is the $M1$ $2_2^+ \rightarrow 2_1^+$ transition. The intrinsic quadrupole moments of all the states are expected to be zero. The values of the g factors of the 2_1^+, 4_1^+, and 2_2^+ states are predicted to be identical and to have the value of $g_{\text{collective}} \simeq Z/A$.

Some of the even-even Cd and Pd isotopes have been among the nuclei that are considered to be the best examples of vibrational nuclei. This evaluation is due, in part, to the observed excitation energies of the low-lying levels. The level schemes clearly display the one-phonon 2_1^+ singlet level and the nearly degenerate two-phonon 4_1^+, 2_2^+, and 0_2^+ triplet levels at about twice the 2_1^+ excitation energy, as shown for ^{106}Pd in Fig. 1(b). Several members of the three-phonon 0_3^+, 2_3^+, 3_1^+, 4_2^+, and 6_1^+ quintuplet have been located [2].

One goal of the present investigation was to test how well the pure vibrational model explains some of the other observed properties, beyond the excitation energy spectrum, of the low-lying states of the supposedly good vibrational ^{106}Pd nucleus.

The ^{106}Pd nucleus was chosen for several reasons. It is stable and isotopically abundant. The ^{106}Pd g factors should be easy to measure, since the excited levels are relatively low lying. In addition, the $g(2_1^+)$ value is a calibration point for the transient field parametrization [3]. Its value, $g = +0.398(21)$ [4,5], was measured in external fields and also by the integral perturbed angular correlation (IPAC) method [6], but needs to be adjusted for a new lifetime, $\tau = 17.6(6)$ ps [2], yielding $g = 0.391(16)$. The g factor of the 2_2^+ state was measured using the IPAC method in two experiments [7,8]. Based on these data and a revised lifetime, a value of $g = +0.30(6)$ was adopted in the compilations by Raghavan [6] and Stone [9].

These particular results and g factors obtained by IPAC or other integral precession measurements depend upon the value of the lifetimes of the relevant states. These lifetimes were deduced from Coulomb excitation experiments and were not independently measured [2,10,11]. In the present investigation, however, lifetimes of the 2_2^+ and 4_1^+ were obtained directly by the Doppler shift attenuation method (DSAM) from the line shapes of the γ transitions. The lifetime of the 2_1^+ state was measured by a plunger experiment [12] and recently remeasured at Yale [13]. In the present work, the $g(2_2^+)$ was remeasured while the $g(4_1^+)$ was measured for the first time.

II. EXPERIMENT

A beam of isotopically pure ^{106}Pd was accelerated in a set of experiments to energies of 230, 280, 290, and 300 MeV at the extended stretched transuranium (ESTU) tandem van de Graff of the Wright Nuclear Structure Laboratory at Yale University. Two multilayer targets were used. Target I consisted of a 0.42-mg/cm^2 carbon layer deposited on a 3.24-mg/cm^2 gadolinium layer that was evaporated onto a 1.4-mg/cm^2 tantalum foil and backed by 3.5-mg/cm^2 copper. A 5-μg/cm^2 titanium flashing was added between the carbon and gadolinium to ensure good adhesion of the carbon. Target II had a 0.606-mg/cm^2 carbon layer deposited on a 6.426-mg/cm^2 gadolinium layer evaporated onto 1.0-mg/cm^2 tantalum and backed by 5.6-mg/cm^2 copper. Additional copper beam stops of 11.2 mg/cm^2 (target I) and 5.6 mg/cm^2 (target II) were placed behind the targets. The Coulomb excitation of the projectiles occurs in the carbon layer. The Coulomb barrier for ^{106}Pd on C is about 374 MeV. The choice of the beam energies resulted from the given target parameters, the desired excitation of the two-phonon states, and the limits of the terminal voltage of the accelerator.

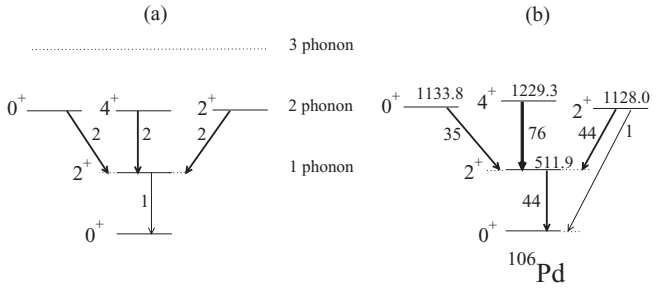

FIG. 1. (a) Predicted excitation energy spectrum and relative $B(E2)$ values (down arrows) for the decay of the lower phonon states within the framework of a harmonic quadrupole vibrator. (b) Energy level diagram of the low-lying states and transitions in ^{106}Pd. The measured $B(E2)$ values are taken from ENSDF [2] and are given in Weisskopf units.

The scattered carbon ions, as well as light particles, which passed though the beam stop, were detected in a passivated, implanted, planar silicon (PIPS) Canberra particle detector positioned at zero degrees with respect to the beam direction, 23 mm downstream of the target and subtending an angle of $\pm 23^\circ$. The γ rays were detected in four segmented high-purity-Ge (HP-Ge) clover detectors located about 130 mm from the target. Two clover detectors (denoted as 2 and 3) were placed at angles of $\pm 67^\circ$ to the beam axis and the other two (denoted as 1 and 4) at $\pm 113^\circ$, as pictured in Ref. [14]. All the particles and γ rays were recorded as singles events in a PIXIE-4 system from XIA [15]. Using the time stamp for each singles event, particle-γ coincidence spectra were constructed offline.

For the precession measurements the target was mounted on the tip of a Displex Closed Cycle cryocooler and kept at a temperature of about 50–60 K. An external field $B_{\rm ext} = 0.07$ T was applied alternately up ($\uparrow$) or down ($\downarrow$) with respect to the γ-ray detection plane; the field direction was changed every 136 s.

A. Data analysis

The energies and velocities of the excited ions that are relevant to the transient field experiment are summarized in Table I.

Figure 2 shows a ^{12}C-γ coincidence spectrum obtained with a ^{106}Pd beam of 300 MeV. Compton-scattered γ rays were added back to the spectra of the individual detector segments. That spectrum shows the relatively weak excitation of the 4_1^+ and 2_2^+ states, a major limiting factor in obtaining accurate values for their g factors.

The precession angle $\Delta\theta = \epsilon/S$ is obtained from the ratios of the γ-peak intensities, $N\uparrow$ and $N\downarrow$, for opposite field directions on the target, which are extracted from the spectra for each individual detector segment. The precession effect $\epsilon = (\rho - 1)/(\rho + 1)$ is calculated from quadruple ratios involving four detectors with the same quadrant angle θ_γ:

$$\rho = \sqrt{\rho_{1,4}/\rho_{2,3}}, \quad \text{where} \quad \rho_{i,j} = \sqrt{(N_i^\uparrow N_j^\downarrow)/(N_i^\downarrow N_j^\uparrow)}. \qquad (1)$$

TABLE I. Summary of the beam energies, the angular momenta and the parity of each excited state, and the kinematics of the recoiling ion. The $\langle E\rangle_{\rm in}$ and $\langle E\rangle_{\rm out}$, and $\langle v/v_0\rangle_{\rm in}$ and $\langle v/v_0\rangle_{\rm out}$ are, respectively, the average energies and velocities of the excited ^{106}Pd ions as they enter into and exit from the gadolinium layer, and $v_0 = e^2/\hbar$ is the Bohr velocity.

$E_{\rm beam}$ MeV	I^π	Target	$\langle E\rangle_{\rm in}$ MeV	$\langle E\rangle_{\rm out}$ MeV	$\langle \frac{v}{v_0}\rangle_{\rm in}$	$\langle \frac{v}{v_0}\rangle_{\rm out}$
230	2_1^+	I	130.1	63.5	7.02	4.90
280	2_1^+	I	163.0	88.2	7.86	5.77
280	2_1^+	II	154.5	34.0	7.63	3.58
290	2_1^+	II	159.6	37.0	7.79	3.75
300	2_1^+	II	166.2	40.3	7.95	3.92
300	2_2^+	II	166.4	40.5	7.96	3.92
300	4_1^+	II	166.4	40.5	7.96	3.92

S is the logarithmic slope of the angular distribution at the detector position. The particle-γ angular correlation

$$W(\theta) = 1 + A_2 Q_2 P_2(\cos\theta) + A_4 Q_4 P_4(\cos\theta) \qquad (2)$$

was determined for each state from anisotropy ratios obtained from the precession data in the individual clover segments as well as from dedicated measurements where each clover detector was placed at angles equivalent to 50° and 80° in each quadrant. The experimental $A_2^{\rm expt}$ and $A_4^{\rm expt}$ coefficients and the logarithmic slopes of the angular distributions $S(\theta_\gamma) = \frac{1}{W(\theta_\gamma)}\frac{dW(\theta_\gamma)}{d\theta}$ were calculated as described in Ref. [16]. The experimentally determined slopes agree with the slopes calculated using the Winther-de Boer COULEX code [17] as adopted in the MuStAng code [18] and are given in Table II for the full clover detectors.

The g factors for each state can then be calculated from the corresponding measured precession angles $\Delta\theta$ using

$$\Delta\theta = -g\frac{\mu_N}{\hbar}\int_{t_{\rm in}}^{t_{\rm out}} B_{\rm TF}[v(t), Z]e^{-t/\tau}dt. \qquad (3)$$

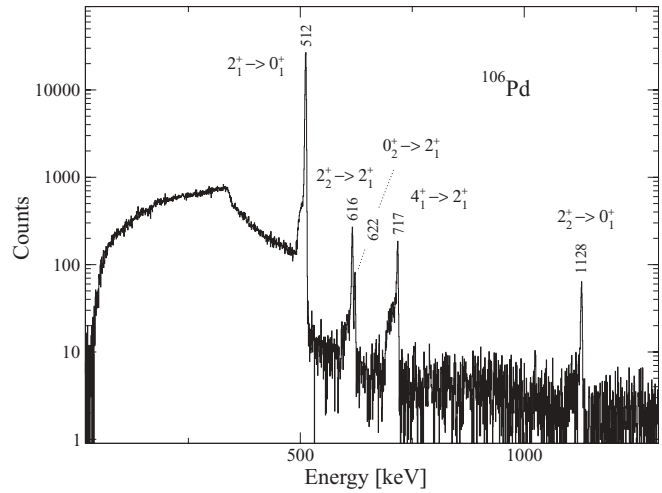

FIG. 2. A ^{12}C-γ coincidence spectrum, with the randoms subtracted, for one clover detector segment at 121°.

TABLE II. Level energy E_x, spin and parity, mean lifetimes, logarithmic slopes $S(\theta_\gamma)$ of the angular correlations at 290 MeV, and deduced g factors.

E_x (keV)	I^π	Transition	τ(ps)		$\lvert S(67^\circ)\rvert$	g		
			This work	Ref. [2]		This work	Refs. [2,6]	Theory[a]
512.85	2_1^+	$2_1^+ \rightarrow 0_1^+$		17.6(6)	1.85(5)		+0.391(16)	+0.5 +0.392[b]
1128.02	2_2^+	$2_2^+ \rightarrow 0_1^+$	4.90(25)	4.50(36)	1.60(13)	+0.48(9)	+0.30(6)	+0.664
1229.30	4_1^+	$4_1^+ \rightarrow 2_1^+$	2.26(10)	1.90(26)	0.86(8)	+0.44(9)		+0.453

[a]This work.
[b]Reference [22].

Here, $B_{\rm TF}$, the transient field, is a function of both the velocity v and the atomic number Z of the projectile ion, and τ is the mean lifetime of the state being considered. The times $t_{\rm in}$ and $t_{\rm out}$ are, respectively, the mean entrance and exit times of the ions into, and out of, the ferromagnetic gadolinium layer.

Likewise, for a given g-factor value, an average $B_{\rm TF}$ can be derived from the measured $\Delta\theta$ using the effective transit time $T = t_{\rm out} - t_{\rm in}$. The transit time is calculated for the reaction kinematics, the lifetime of the state, and the energy loss $\frac{dE}{dx}$ of the ions in the ferromagnetic layer. The average $B_{\rm TF}$ strength is given by

$$B_{\rm TF} = \frac{\Delta\theta}{(\mu_N/\hbar) g T \mathrm{M}}, \tag{4}$$

where M denotes the percentage of the full magnetization of the target. The magnetization $\vec{M}$ of a target is measured offline in an ac magnetometer [19] at temperatures ranging from 10 to 300 K. The largest magnetization for a given magnetizing field is observed for $50 < T < 100$ K. Typical gadolinium foils have, in this temperature range, a constant magnetization of about 80% of the full bulk magnetization of 0.2116 T. Above 120 K, the magnetization of gadolinium falls off rapidly as a function of increasing temperature and vanishes at room temperature [20].

In Fig. 3 the measured average $B_{\rm TF}$ is shown for the two targets and applied beam energies. The horizontal "error" bars show the velocity range of the probe ions within the ferromagnetic layer. According to the Rutgers transient field parametrization [3],

$$B_{\rm TF}[v(t), Z] = a Z^{1.1} \left(\frac{v}{v_o}\right)^{0.45} M, \tag{5}$$

the field should increase with velocity as shown by the line in the graph.

B. Beam power and target magnetization

In the presentation of Fig. 3, all measurements would be expected to give about the same transient field strength since they correspond to a relatively narrow velocity range. However, the actual measured fields vary strongly from experiment to experiment. For target II the observed field strength at higher beam energies (velocities) is consistently lower, although the parametrization [Eq. (5)] predicts an increase with velocity. According to Eq. (5), the lower results can only be caused by a reduction of the magnetization of the target in beam.

When the beam is fully stopped in the target, a power of 0.2–0.3 W is deposited in the beam spot (diameter of 2.5 mm). Although the target is cooled to 50 K by a Displex Closed Cycle cryocooler system, the actual temperature of the beam spot is not known. Depending on beam energy and beam current density (beam focus) the beam-spot temperature can fluctuate locally, and, if it exceeds 120 K, the measured precession effect will be significantly reduced. The lowest point in Fig. 3 was obtained at a beam energy of 300 MeV (target II, $M = 0.1780$ T) and with beam currents as low as 1 pnA. Also in this experiment, a connection between beam load, target temperature setting, and measured effect was clearly established. The highest point was obtained at a lower beam energy and a slightly lower beam intensity. But that result was obtained only after an additional cooling shield, which was kept at 50 K, was mounted, surrounding the target, in order to improve the radiative cooling of the target beam spot. In a later run with ^{106}Pd at 290 MeV, in spite of using the cooling shield around the target, a statistically significant reduced effect was measured. The square data points in Fig. 3 were measured with target I ($M = 0.1860$ T). At 230 MeV, the

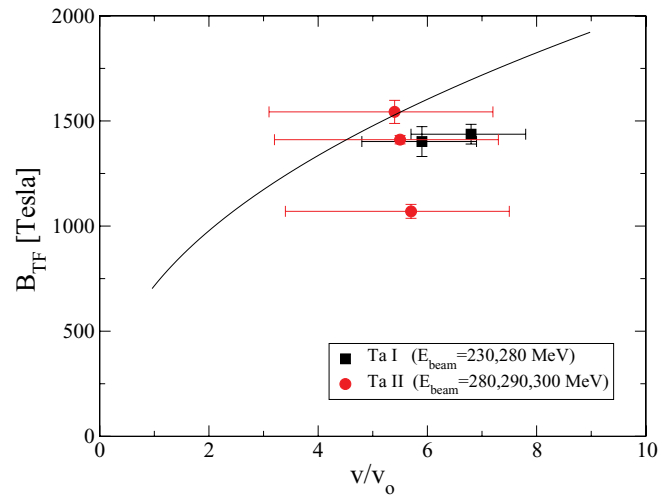

FIG. 3. (Color online) Average transient fields as measured in these experiments. The $B_{\rm TF}$ is calculated for $g = 1$ and 100% magnetization. The line represents the Rutgers parametrization for a $g = +0.52$.

beam load should be lowest; yet at 280 MeV the same value of the field was obtained although the probe ion velocity was distinctly larger, again implying a reduction in M.

Former experiments at lower beam energies and low currents did not exhibit these effects. This observation may be explained by the fact that the reduction in the magnetization acts like a threshold effect. As long as the equilibrium temperature of the target beam spot, which results from a balance between the power deposition and the heat dissipation, stays below 120 K, the magnetization remains high and constant. Once this condition is exceeded the results are unpredictable.

C. Results

Since the Rutgers parametrization [Eq. (5)] explicitly includes M, it cannot be used to extract a g factor unless the in-beam magnetization is stable and reliably known. The parametrization for the highest point in Fig. 3, assuming that the offline measured magnetization applies, results in a $g(2_1^+)$ factor for ^{106}Pd of $+0.52$, a value much higher than the adopted calibration value. The average of all measurements shown in Fig. 3, except for the 300-MeV data where a reduction of the effect with beam power was clearly established, yields $g(2_1^+;^{106}\,\mathrm{Pd}) = +0.48(1)$. This result is still in disagreement with the calibration value. At the current status of the present investigation, no simple explanation can be offered for this discrepancy. Obtaining too "high" a value for the transient field is remarkable since any experimental problem would only lead to a reduction of the measured effects. There are two possible explanations: either, according to Eq. (5), the so-called strength factor a in the Rutgers parametrization for gadolinium should be larger, or else the g-factor results of the IPAC measurements, for some reason, are too low. Both options are unsatisfactory.

A detailed experimental study of the beam-power-related effects is underway, focusing especially on a comparison between gadolinium ($T_{Curie} \sim 300$ K) and iron ($T_{Curie} = 1043$ K) ferromagnets.

The value of $g(^{106}\mathrm{Pd};2_1^+)$ was measured by H. T. King *et al.* [21] by the transient field technique in gadolinium and iron. Their precession results have relatively large errors and agree with both the IPAC g-factor value and the g factor measured here.

Nevertheless, in the present work the relative g factors of the three states were measured simultaneously and are not affected by the above considerations. Using the measured precession angle of the 2_1^+ state and the calibration g factor of $+0.391(16)$, B_{TF} in the Rutgers parametrization [Eq. (5)] was adjusted by scaling the in-beam magnetization M. The g factors for the 4_1^+ and 2_2^+ states were then calculated using this value of M in Eq. (3). The results are summarized in Table II.

The lifetimes of the 4_1^+ and 2_2^+ states were newly determined using the DSAM technique and the LINESHAPE code [23]. A modified Monte Carlo code, that takes into account the triple layer target and uses Ziegler's stopping-power tables [24] was used to calculate a set of decay histories for the line shapes to be fitted. The large probe ion recoil velocities from the inverse kinematics reaction (see Table I) allow for sensitive life time

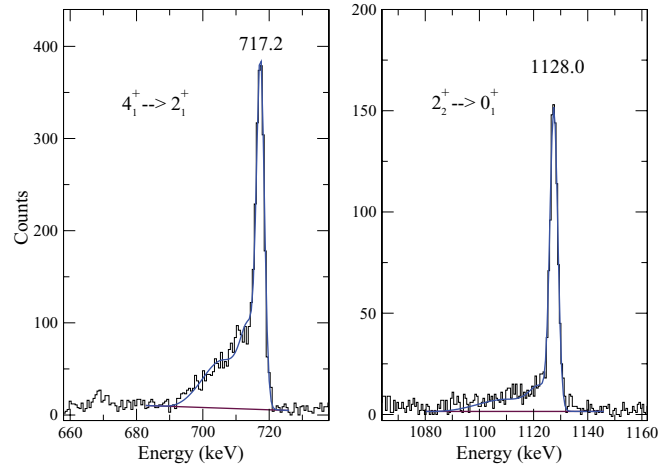

FIG. 4. (Color online) Line-shape fits for the 4_1^+ and 2_2^+ states.

measurements [25]. The line-shape fits were performed for the data of single clover segments located at forward and backward angles. Figure 4 shows the fitted data for $\theta = 121°$. The results are presented in Table II. The new lifetimes are slightly larger than those previously reported. The longer lifetime that is reported here for the 2_2^+ state would make the $g(2_2^+)$ factor derived from the the IPAC measurement [6] even smaller.

III. DISCUSSION

The new data of the present experiment can now be incorporated into an overall analysis of how well the pure vibrational model accounts for the observed properties of the low-lying levels of ^{106}Pd. Such an approach was taken earlier in Ref. [26]. Figure 1(a) displays the predictions of the pure harmonic quadrupole-phonon vibrator picture. Figure 1(b) presents experimental data for the ^{106}Pd nucleus.

The observed low-lying excitation energy spectrum in Fig. 1(b) does bear a strong resemblance to the vibrational model picture. The one-phonon singlet and the two-phonon triplet are evident, with the three two-phonon states separated by only 101 keV. The center of mass of the triplet lies at 1163.7 keV, while the I-weighted center of mass lies at 1189.2 keV. These values are ~2.3 times larger than the single-phonon $E(2_1^+)$ excitation energy; the pure vibrational model predicts a ratio of 2 for the excitation energy of the triplet to that of the singlet.

The $B(E2)$ values corresponding to a transition with a one-phonon change are all between 35 and 76 Weisskopf units (W.u.), indicating the collectivity that the vibrational model predicts. The $B(E2;\, 2_2^+ \rightarrow 0_1^+)$ two-phonon transition, forbidden in the pure vibrational model, is much smaller at 1.2 W.u.. The vibrational model predicts that the $B(E2)$ value for the transition from each of the two-phonon states to the one-phonon state should be twice the $B(E2;\, 2_1^+ \rightarrow 0_1^+)$ value. The actual values and ratios are shown in Table III and the ratios are clearly less than two. That the ratio $B(E2;\, 0_2^+ \rightarrow 2_1^+)/B(E2;\, 2_1^+ \rightarrow 0_1^+)$ is much smaller than the vibrational-model prediction was noted by Garrett, Green, and Wood [27] for the Cd isotopes, especially for ^{116}Cd. These

TABLE III. Summary of spectroscopic information.

Transition $I_f \to I_f$	$2_1^+ \to 0_1^+$	$2_2^+ \to 0_1^+$	$2_2^+ \to 2_1^+$	$4_1^+ \to 2_1^+$	$0_2^+ \to 2_1^+$
Branching Ratio[b]		35.2	64.8		
$\delta\left(\frac{E2}{M1}\right)$[b]			−9.4(20)		
τ[ps]	17.6(6)[b]	4.90(25)[a]		2.26(10)[a]	8.37(188)[b]
$B(M1)$ [W.u.][b]			0.00022		
$B(E2)$ [W.u.][b]	44	1.2	44	76	35
$B(E2)$ [e^2b^2]	0.131	0.0036	0.131	0.227	0.104
$\frac{B(E2;\, I_f \to I_f)}{B(E2;\, 2_1^+ \to 0_1^+)}$	1.00	0.03	1.00	1.73	0.80

[a]This work.
[b]Reference [2].

authors considered this result a definite challenge to the pure vibrational model.

The g-factor values for the 2_1^+, 2_2^+, and 4_2^+ levels are all predicted by the vibrational model to be $g \simeq Z/A = +0.433$. The adopted $g(2_1^+)$ value is, within errors, only about 3% from the collective value. The $g(2_2^+)$ and the $g(4_1^+)$ values agree, within error, with both the Z/A prediction and the adopted $g(2_1^+)$ value. The $g(2_2^+)$ value is larger than the previously adopted value.

It is interesting to note that the present investigations indicate that the pure vibrational model does account, within the experimental errors, for the experimental g factors of the low-lying states of the ^{106}Pd nucleus. Such is not the case for the $B(E2)$ transition strengths.

The set of results discussed in the preceding paragraph can be explained by phonon-mixing along the lines suggested in [28]. The wave function Ψ of the observed state can thus be assumed to consist of two orthogonal components ϕ and χ with different fixed phonon numbers

$$\Psi = a\phi + b\chi \tag{6}$$

and $a^2 + b^2 = 1$.

Each component can be assumed to have the same g factor regardless of its phonon number. Thus the mixed-phonon states will also all have the same g factor of Z/A. However, the $B(E2)$ transition strength between two pure phonon states, say with respective phonon numbers $N+1$ and N, depends on the value of N. Hence the $B(E2)$s of the mixed-phonon states would differ from the predictions of the pure vibrational model.

It can be shown that the $B(M1)$s between such mixed-phonon states vanish, just as they do between pure phonon states.

If, however, the mixing occurs between vibrational states and nonvibrational intruder states (see Ref. [27]), then the above line of reasoning will not apply. But it should be noted that the intruder states in ^{106}Pd are considerably further away in their excitation energies from the excitation energies of the two-phonon states in ^{106}Pd than is the case in the Cd isotopes considered in Ref. [27].

The static quadrupole moment of the 2_1^+ state in ^{106}Pd has been measured in several previous experiments to be $Q(2_1^+) = -0.56(8)$ b [28], $-0.41(8)$ b or $-0.51(7)$ b [29], and $-0.458(59)$ b or $-0.282(59)$ b, depending on the signs of interference effects [30]. These values disagree with the $Q(2_1^+) = 0$ prediction of the pure vibrational model.

The National Nuclear Data Center (NNDC) database reports a value of $B(M1)$ from the $2_2^+ \to 2_1^+$ state of 0.00022(10) W.u. based on Ref. [26]. This very small value is consistent with the pure quadrupole-phonon vibrational model in which such an $M1$ transition is forbidden.

A shell-model calculation for ^{106}Pd was carried out using the JJ45PN interaction of Brown and Hjorth-Jensen [31]. This calculation utilized a closed core of $Z = 28$ protons and $N = 50$ neutrons. The four proton holes could be anywhere in the $f_{5/2}$, $p_{3/2}$, $p_{1/2}$, $g_{9/2}$ space. The ten neutrons were confined to the $g_{7/2}$, $d_{5/2}$ space. The single-particle energies used in that calculation were based on data for nuclei near ^{132}Sn.

The shell-model results for the g factors of the 2_1^+, 2_2^+, and 4_1^+ states are shown in Table II. The calculated $g(2_2^+)$ value is larger than the other two calculated g-factor values, while the $g(2_1^+)$ is overestimated by 25% compared to the measured value. However, in this particular shell-model calculation the excitation energies in the ^{106}Pd nucleus are overpredicted by a factor of about 1.4; the calculated $B(E2)$ values (using $e_p = 1.5e$ and $e_n = 0.5e$) are underpredicted by factors of 6 to 10, a problem which can be only partially resolved by using larger effective charges and which may be due, in part, to the choice of single-particle energies. These results indicate that, in the shell-model space that was utilized, the calculations strongly underpredict the collectivity of the ^{106}Pd nucleus. This perspective is borne out by the very fractionated nature of the shell-model wave functions for the states of ^{106}Pd. For example, the probability of the largest shell-model configuration component in the wave function of the 0_1^+, 0_2^+, 2_1^+, and 2_2^+ states is only 12%, 28%, 13%, and 17%, respectively.

All of the above calculated shell-model results suggest that a more collective approach is required to understand the structure of the ^{106}Pd nucleus. In Ref. [22] Kim *et al.* carried out an IBM-2 calculation for this nucleus. They consider ^{106}Pd to be in the U(5) to O(6) transitional region and find values for the excitation energies and electromagnetic $E(2)$ transition strengths. Their results agree well with the experimental data (see Table III and Fig. 3 in Ref. [22]). They calculate the $g(2_1^+)$ factor to be $+0.392$, in excellent agreement with the experimental data, but do not calculate any other g factors.

IV. SUMMARY

The excitation of the two-phonon states was weak and required higher beam energies. These higher beam energies led to more power deposition on the target and to fluctuations in the precession measurements. The reductions in the observed precession effect were correlated with the increased beam power and hence a possibly enhanced beam-spot temperature. So far there is no suitable way to monitor the beam-spot temperature. In addition to the cold shield around the target, a larger beam-spot diameter will be used in future experiments. Despite a reduced magnetization for some of the measurements, the TF-derived g factor for the 2_1^+ is larger than the old IPAC measurements. In this publication the IPAC g-factor value was used as the standard value to which all other measurements were normalized.

In this work it was shown that the measured g factors of the one-phonon and two-phonon states in ^{106}Pd agree with the simple vibrational model. That model also accounts well for the excitation energies of these levels. A mixed-phonon perturbation to the vibrational states could perhaps explain the observed $B(E2)$ ratios in ^{106}Pd but cannot explain the measured nonzero static quadrupole moment of the 2_1^+ state in this nucleus.

The shortcomings of the shell-model calculational results indicate the collective nature of this nucleus. The results of Kim *et al.* suggest that ^{106}Pd can be best understood not in a pure U(5) vibrational picture, but rather within a transitional picture between the U(5) and O(6) limits in the IBM-2.

ACKNOWLEDGMENTS

The authors are indebted to the staff of the Wright Nuclear Science Laboratory for their assistance during the experiment. The targets used in this experiment were prepared by Dr. P. Maier-Komor (Physik-Department der Technischen Universität München, D-85748 Garching, Germany). Y.Y.S. is grateful to the Richard Sockton College of New Jersey for a Sabbatical Grant. S.J.Q.R. acknowledges a Travel Grant from Millsaps College. The work was supported in part by the US National Science Foundation and the US Department of Energy under Grant DE-FG02-91ER-40609.

[1] G. Scharff-Goldhaber and J. Weneser, Phys. Rev. **98**, 212 (1955).
[2] D. D. Frenne and A. Negret, Nucl. Data Sheets **109**, 943 (2008).
[3] N. K. B. Shu, D. Melnik, J. M. Brennan, W. Semmler, and N. Benczer-Koller, Phys. Rev. C **21**, 1828 (1980).
[4] K. Auerbach, K. Siepe, J. Wittkemper, and H. J. Körner, Phys. Lett. **23**, 367 (1966).
[5] K. Johansson, E. Karlsson, L.-O. Norlin, R. A. Windahl, and M. R. Ahmed, Nucl. Phys. A **188**, 600 (1972).
[6] P. Raghavan, At. Data Nucl. Data Tables **42**, 189 (1989).
[7] J. D. Bowman, E. N. Kaufmann, S. K. Bhattacherjee, and M. Levanoni, Phys. Rev. Lett. **20**, 1176 (1968).
[8] V. Singh, J. Phys. Soc. Jpn. **29**, 1111 (1970).
[9] N. Stone, *Table of New Nuclear Moments* (Oxford University, 1997).
[10] P. Stelson and F. McGowan, Phys. Rev. **121**, 209 (1961).
[11] Y. P. Gangrksii and I. K. Lemberg, Sov. Phys. JETP **15**, 711 (1962).
[12] M. Loiselet, O. Naviliat-Cuncic, and J. Vervier, Nucl. Phys. A **496**, 559 (1989).
[13] G. Ilie (to be published).
[14] P. Boutachkov *et al.*, Phys. Rev. C **76**, 054311 (2007).
[15] X-Ray Instrumentation Associates [http://www.xia.com/].
[16] N. Benczer-Koller and G. J. Kumbartzki, J. Phys. G: Nucl. Part. Phys. **34**, R321 (2007).
[17] A. Winther and J. de Boer, *A Computer Program for Multiple Coulomb Excitation* (Academic Press, New York, 1966).
[18] A. E. Stuchbery, *Computer code MuStAng* (2004), ANU, Canberra ACT 0200, Australia.
[19] A. Piqué, J. M. Brennan, R. Darling, R. Tanczyn, D. Ballon, and N. Benczer-Koller, Nucl. Instrum. Methods Phys. Res. A **279**, 579 (1989).
[20] R. S. Trebble and D. J. Craik, *Magnetic Materials* (Wiley & Sons, Ltd, London, 1969).
[21] H. T. King, D. L. Clark, and J. S. Dunham, Phys. Rev. B **25**, 1497 (1982).
[22] K. H. Kim, A. Gelberg, T. Mizusaki, T. Otsuka, and P. von Brentano, Nucl. Phys. A **604**, 163 (1996).
[23] J. C. Wells and N. R. Johnson, *Computer code* LINESHAPE (1999), PD-LNL version.
[24] F. J. Ziegler, J. Biersack, and U. Littmark, *The Stopping and Range of Ions in Solids* (Pergamon, Oxford, 1985), Vol. I.
[25] R. Ernst *et al.*, Phys. Rev. C **62**, 024305 (2000).
[26] L. E. Svensson, C. Fahlander, L. Hasselgren, A. Bäcklin, L. Westerberg, D. Cline, T. Czosnyka, C. Y. Wu, R. M. Diamond, and H. Kluge, Nucl. Phys. A **584**, 547 (1995).
[27] P. E. Garrett, K. L. Green, and J. L. Wood, Phys. Rev. C **78**, 044307 (2008).
[28] K. Hosoyama, Y. Torizuka, Y. Kawazoe, and H. Ui, Phys. Rev. Lett. **30**, 388 (1973).
[29] W. R. Lutz, J. A. Thomson, R. P. Scharenberg, and R. D. Larsen, Phys. Rev. C **6**, 1385 (1972).
[30] R. Beyer, R. P. Scharenberg, and J. Thomson, Phys. Rev. C **2**, 1469 (1970).
[31] M. Hjorth-Jensen, T. Kuo, and E. Osnes, Phys. Rep. **261**, 125 (1995).